


# *L*-shell x-ray fluorescence relative intensities for elements with $62 \leq Z \leq 83$ at 18 keV and 23 keV by synchrotron radiation

M Alqadi, S AL-Humaidi, H Alkhateeb, and F Alzoubi

**Citation:**Chin. Phys. B, 2023, 32 (**8**): 083201. DOI: 10.1088/1674-1056/accb46
Journal homepage: http://cpb.iphy.ac.cn; http://iopscience.iop.org/cpb

**What follows is a list of articles you may be interested in**

---

## Electron emission induced by keV protons from tungsten surface at different temperatures

Li-Xia Zeng(曾利霞), Xian-Ming Zhou(周贤明), Rui Cheng(程锐), Yu Liu(柳钰), Xiao-An Zhang(张小安), and Zhong-Feng Xu(徐忠锋)
Chin. Phys. B, 2022, 31 (**7**): 073202. DOI: 10.1088/1674-1056/ac632f

## Nd *L*-shell x-ray emission induced by light ions

Xian-Ming Zhou(周贤明), Jing Wei(尉静), Rui Cheng(程锐), Yan-Hong Chen(陈燕红),Ce-Xiang Mei(梅策香), Li-Xia Zeng(曾利霞), Yu Liu(柳钰), Yan-Ning Zhang(张艳宁), Chang-Hui Liang(梁昌慧), Yong-Tao Zhao(赵永涛), and Xiao-An Zhang(张小安)
Chin. Phys. B, 2022, 31 (**6**): 063204. DOI: 10.1088/1674-1056/ac4488

## X-ray emission for $Ar^{11+}$ ions impacting on various targets in the collisions near the Bohr velocity

Xian-Ming Zhou(周贤明), Jing Wei(尉静), Rui Cheng(程锐), Yan-Hong Chen(陈燕红), Ce-Xiang Mei(梅策香), Li-Xia Zeng(曾利霞), Chang-Hui Liang(梁昌慧), Yao-Zong Li(李耀宗), Yong-Tao Zhao(赵永涛), and Xiao-An Zhang(张小安)
Chin. Phys. B, 2021, 30 (**8**): 083201. DOI: 10.1088/1674-1056/abe22f

## Extreme ultraviolet and soft x-ray spectral lines in Rb XXIX

Indu Khatri, Arun Goyal, Sunny Aggarwal, A K Singh, Man Mohan
Chin. Phys. B, 2016, 25 (**3**): 033201. DOI: 10.1088/1674-1056/25/3/033201

## Broadband time-resolved elliptical crystal spectrometer for X-ray spectroscopic measurements in laser-produced plasmas

Wang Rui-Rong (王瑞荣), Jia Guo (贾果), Fang Zhi-Heng (方智恒), Wang Wei (王伟), Meng Xiang-Fu (孟祥富), Xie Zhi-Yong (谢志勇), Zhang Fan (张帆)
Chin. Phys. B, 2014, 23 (**11**): 113201. DOI: 10.1088/1674-1056/23/11/113201

---

# *L*-shell x-ray fluorescence relative intensities for elements with $62 \leq Z \leq 83$ at 18 keV and 23 keV by synchrotron radiation

M Alqadi[†], S AL-Humaidi, H Alkhateeb, and F Alzoubi

*Department of Physics, Jordan University of Science and Technology, Irbid, Jordan*

(Received 25 January 2023; revised manuscript received 3 April 2023; accepted manuscript online 7 April 2023)

The relative intensities of *L*-subshell x-ray fluorescence (XRF) for elements with atomic numbers $62 \leq Z \leq 83$ were measured at two excitation energies, 18 keV and 23 keV, using a synchrotron radiation source at a beamline of the Synchrotron Light Center for Experimental Science and Applications in the Middle East (SESAME), Jordan. The experimentally measured results of the relative intensities were compared with the calculated results using the subshell fluorescence yield and the Coster–Kronig transition probabilities recommended by Campbell and the values based on the Dirac–Hartree–Slater model by Puri. The experimental and theoretical results are in agreement. In this work, *L* XRF relative intensities for the elements Sm, Gd, Tb, Er, Ta, W, Re, Hg, Pb and Bi at energies of 18 keV and 23 keV were measured.

**Keywords:** *L* shell, x-ray fluorescence (XRF), relative intensities, synchrotron radiation

**PACS:** 32.30.Rj, 32.50.+d, 32.70.Fw, 32.80.Fb **DOI:** 10.1088/1674-1056/accb46

## 1. Introduction

Precise determination of the fundamental parameters is essential in a variety of fields of physics, for example, dose calculation in medical physics, non-destructive quantitative analysis, atomic physics, molecular physics, radiation physics and the development of more accurate theoretical models to explain inner-shell ionization processes.[1] The theoretical x-ray fluorescence (XRF) cross section and intensities can be determined using fundamental parameters: the fraction emission, *K*-, *L*- and *M*-subshell fluorescence yields, photoionization cross sections and Coster–Kronig (CK) transition probabilities. The uncertainty in the theoretical values of fundamental parameters, in particular the CK transition probabilities and subfluorescence yields, is reflected in the values of the XRF cross sections and their relative intensities. Therefore the experimental values of the XRF cross sections and the relative intensities are used when there are significant differences between theoretical and experimental results. Moreover, it is important to compare the measured data of the *L*-shell line intensities with the theoretical values to investigate correct fundamental parameter sets.

Many studies have reported the measurements as well as the theoretical calculations of *K*- and *L*-shell XRF relative intensities for different elements at different excitation energies using various energy sources such as x-ray tubes, radioisotopes, synchrotron radiation and secondary targets as excitation sources.

Using a radioisotope source, Darko *et al.*[2] reported the intensity ratios for seven elements (Sm, W, Ir, Au, Hg, Pb and U) at an excitation energy of 22.6 keV. The results were compared with Scofield's theoretical values and agreed upon in most cases. Rao *et al.*[3] used a secondary target as an excitation source and a Si(Li) detector to measure the *L* x-ray intensity ratios for Au and Pb at three photoexcitation energies (21.56 keV, 31.64 keV and 34.17 keV). Demir *et al.*[4] measured the *L* XRF cross sections and relative intensities in the atomic range $78 \leq Z \leq 92$. Alqadi *et al.*[5] determined the *L*-shell x-ray relative intensities for Bi, Pr, Pt, Hg and Ba at an excitation energy of 20.48 keV. Bansal *et al.*[6] reported the intensity ratios for elements in the atomic range $66 \leq Z \leq 83$ using synchrotron radiation. Using an x-ray tube source, Ganly *et al.*[7] reported the measurements of the relative total *L*-subshell x-ray intensities for the elements Er, Tm, Yb, Hf, Ta, W, Pt and Au using monoenergetic x-rays at 17.4 keV. Likewise, Hiremath *et al.*[8] measured *L*-subshell XRF yield ratios and the x-ray intensities of some heavy elements (Hf, Ta and Re) using microprobe synchrotron radiation and detected the emitted *L*-shell XRF photons with a silicon drift detector.

In this work, we measured the Lsubshell XRF relative intensities for elements with atomic numbers $62 \leq Z \leq 83$ at two excitation energies, 18 keV and 23 keV, using synchrotron radiation at the Synchrotron Light Center for Experimental Science and Applications in the Middle East (SESAME), Jordan. Our experimental results are compared with theoretical calculated values using the recommended values of the subshell fluorescence yield ($\omega_{Li}$) and the CK transition probabilities ($f_{ij}$) of Campbell[9] and the values based on the Dirac–Hartree–Slater model by Puri *et al.*[10] To our knowledge, *L* XRF relative intensities for the elements Sm, Gd, Tb, Er, Ta, W, Re, Hg, Pb and Bi at energies of 18 keV and 23 keV are reported here for the first time.

[†]Corresponding author. E-mail: malqadi@just.edu.jo

© 2023 Chinese Physical Society and IOP Publishing Ltd 

## 2. Experiment

The experiment was conducted using the XRF beamline at SESAME, Jordan. The synchrotron radiation is collimated by a double-coated (Si and Pt) mirror. To convert the radiation to monochromatic x-rays, a double-crystal monochromator (DCM) (Si(111) or Si(311)) is used. The beam size is about 0.4 mm×0.4 mm, which is achieved using vertically focusing mirror. The XRF beamline provides a tunable x-ray source over an energy range from 4.7 keV to 30 keV[11] (Fig. 1(a)).

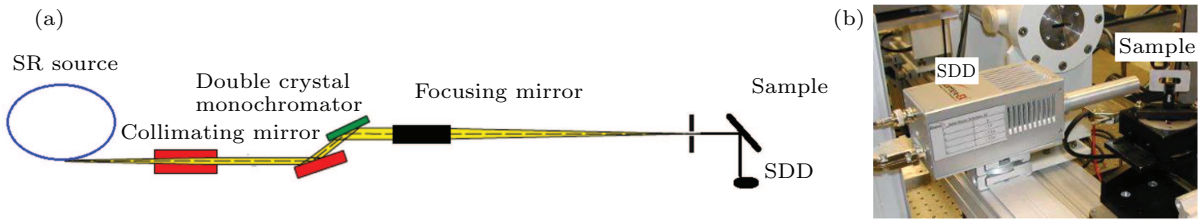



**Fig. 1.** (a) Diagram of the optical layout of the XRF beamline. (b) The experimental set-up.

The irradiated sample was held at an angle of 45° to the incident beam in a horizontal plane. Fluorescence radiation emitted from the sample was detected using a KETEK silicon drift detector with an energy resolution of 138 eV at 5.96 keV Fe $K\alpha$ x-rays and was positioned at an angle of 90° to the incident beam (Fig. 1(b)).

The Sm, Gd, Tb, Er, Ta, W, Re, Pb, Bi, Ti, Cr, Fe, Ni, Cu and Zr metal plates used in this study were purchased with a purity of 99.99% from Alfa Aesar and Sigma Aldrich. Two samples, Ge and $Hg_2Cl_2$, were prepared from powder and pressed into 10 mm diameter pellets using a 15 ton hydraulic press.

## 3. Theoretical $L$ XRF relative intensities

The values of the intensities $I(L_i)$ for the different lines in the $L$ x-ray spectrum are calculated theoretically using the relationships proposed by Close *et al.*[12]

$$I(L_l) = (\sigma_{L1}f_{13}+\sigma_{L1}f_{12}f_{23}+\sigma_{L2}f_{23}+\sigma_{L3})\omega_3 F_{3l}, \quad (1)$$

$$I(L_\alpha) = (\sigma_{L1}f_{13}+\sigma_{L1}f_{12}f_{13}+\sigma_{L2}f_{23}+\sigma_{L3})\,\omega_3 F_{3\alpha}, \quad (2)$$

$$I(L_\beta) = \sigma_{L1}\omega_1 F_{1\beta}+(\sigma_{L2}+\sigma_{L1}f_{12})\omega_2 F_{2\beta} + (\sigma_{L1}f_{13}+\sigma_{L1}f_{12}f_{23}+\sigma_{L2}f_{23}+\sigma_{L3})\omega_3 F_{3\beta}, \quad (3)$$

$$I(L_\gamma) = \sigma_{L1}\omega_1 F_{1\gamma}+(\sigma_{L2}+\sigma_{L1}f_{12})\omega_2 F_{2\gamma}, \quad (4)$$

where $\sigma_{L1}$, $\sigma_{L2}$ and $\sigma_{L3}$ are the non-relativistic Hartree–Fock–Slater based model photoionization cross sections of $L$ subshells $L_1$, $L_2$ and $L_3$, respectively,[13] $\omega_1$, $\omega_2$ and $\omega_3$ are the Lsubshell fluorescence yields, $f_{12}$, $f_{13}$ and $f_{23}$ are the CK transition probabilities. $F_{nx}$ is the fractional radiative emission rate calculated using the Dirac–Fock model based radiative transition rates of Scofield.[15]

Two sets of XRF cross sections are calculated at 18 keV and 23 keV. The first set of XRF cross sections is calculated using the recommended values of fluorescence yield ($\omega_{Li}$) and the CK transition probabilities ($f_{ij}$) of Campbell,[9] who compiled the experimental values of $\omega_i$ and $f_{ij}$ and compared them with the predictions of the relativistic Dirac–Hartree–Slater (RDHS) model and the tabulated values of Krause *et al.*[14] The second set uses Puri values derived from radiative and non-radiative transition rates based on the RDHS model to calculate fluorescence yields and CK transition probabilities.[10]

## 4. Data analysis

The measured experimental values of relative intensity were calculated by

$$\frac{I(L_j)}{I(L_\alpha)} = \frac{N(L_j)\,T(L_\alpha)\,\varepsilon(L_\alpha)}{N(L_\alpha)\,T(L_j)\,\varepsilon(L_j)}, \quad (5)$$

where $N(L_\alpha)$ and $N(L_j)$ are the counts per time under the $L_\alpha$ and $L_j$ ($j=\beta$, $\gamma$, $l$) peaks, respectively. $T(L_j)$ and $T(L_\alpha)$ are the self-attenuation correction factors of the target for the $L_j$ and $L_\alpha$ x-ray energies, respectively, which are given by

$$T_i = \frac{1-\exp(-(\mu(E_\mathrm{i})\sec\theta_1+\mu(E_\mathrm{e})\sec\theta_2)\rho d)}{(\mu(E_\mathrm{i})\sec\theta_1+\mu(E_\mathrm{e})\sec\theta_2)\rho d}, \quad (6)$$

where $\rho$ and $d$ are the density and thickness of the target and $\mu(E_\mathrm{i})$ and $\mu(E_\mathrm{e})$ are the mass attenuation coefficients ($\mathrm{cm^2\cdot g^{-1}}$) at the incident photons and the fluorescent emitted x-ray energies, respectively. The values of mass attenuation coefficients were taken from NIST XCO.[17] $\varepsilon(L_\alpha)/\varepsilon(L_j)$ is the ratio of the efficiency values of the detector at energies corresponding to $L_\alpha$ and $L_j$ energies calculated using

$$\frac{\varepsilon(L_\alpha)}{\varepsilon(L_j)} = \frac{I_0 G\varepsilon(L_\alpha)}{I_0 G\varepsilon(L_j)}. \quad (7)$$

The $I_0G\varepsilon$ factor, which includes the intensity of the incident energy $I_0$, the geometric factor $G$ and the efficiency $\varepsilon$, was calculated from $K$ x-ray peaks for Ti, Cr, Fe, Ni, Cu, Ge and Zr using theoretical XRF cross section values of the K shell ($\sigma_{k\alpha}$ and $\sigma_{k\beta}$) according to

$$I_0 G\varepsilon_{ki} = \frac{N_{ki}}{\sigma_{ki}t\beta_{ki}}, \quad (8)$$

where $N_{ki}$ $(i=\alpha,\beta)$ represents the area under the $K_i$ peak and $\sigma_{ki}$ is the XRF cross section for $K_i$ x-ray lines calculated by

$$\sigma_{k\alpha}=\sigma_k(E)\,\omega_k F_{k\alpha},\quad \sigma_{k\beta}=\sigma_k(E)\,\omega_k F_{k\beta}. \tag{9}$$

Here $\sigma_k(E)$ is the photoionization cross section[13] and $F_{k(\alpha,\beta)}$ are the fractional emission rates for $K$-shell x-rays.[15]

**Table 1.** Values of fitted coefficients at 18 keV and 23 keV.

| Energy (keV) | $a_0$ | $a_1$ | $a_2$ |
|---|---|---|---|
| 18 | 370.79 | –14.17 | 0.179 |
| 23 | 290.03 | 37.64 | –1.90 |

The $I_0G\varepsilon$ values for $L$-shell x-ray energy were estimated using the fitted curve based on the fitting equation

$$I_0G\varepsilon(E)=a_0+a_1E+a_2E^2, \tag{10}$$

where $E$ is the energy of the x-rays and $a_0$, $a_1$ and $a_2$ are constants. Their values are given in Table 1.

## 5. Results and discussion

The XRF relative intensities $I(L_l/L_\alpha)$, $I(L_\beta/L_\alpha)$ and $I(L_\gamma/L_\alpha)$ for the elements Sm, Gd, Tb, Er, Ta, W, Re, Hg, Pb and Bi were measured at two excitation energies (18 keV and 23 keV) using synchrotron radiation. The experimental results are listed in Tables 2 and 3. These tables also show the theoretical values of relative intensities which are calculated using the $\omega_i$ and $f_{ij}$ values of Campbell[9] and the calculated values of Puri *et al.*[10] using Eqs. (1)–(4).

**Table 2.** Comparing the experimental results of relative intensities with theoretical values at an excitation energy of 18 keV.

| $Z$ | $I(L_\beta/L_\alpha)$ | | | $I(L_\gamma/L_\alpha)$ | | | $I(L_l/L_\alpha)$ | | |
|---|---|---|---|---|---|---|---|---|---|
| | Present experiment | Puri[10] | Campbell[9] | Present experiment | Puri[10] | Campbell[9] | Present experiment | Puri[10] | Campbell[9] |
| 62 | 1.119±0.09 | 1.057 | 1.089 | 0.031±0.008 | 0.040 | 0.041 | 0.202±0.027 | 0.191 | 0.187 |
| 64 | 1.277±0.09 | 1.066 | 1.111 | 0.038±0.009 | 0.041 | 0.041 | 0.238±0.028 | 0.193 | 0.194 |
| 65 | 1.301±0.10 | 1.066 | 1.130 | 0.036±0.01 | 0.041 | 0.042 | 0.237±0.03 | 0.191 | 0.194 |
| 68 | 1.240±0.08 | 1.053 | 1.091 | 0.041±0.008 | 0.043 | 0.043 | 0.227±0.023 | 0.190 | 0.186 |
| 73 | 1.187±0.07 | 1.082 | 1.080 | 0.039±0.006 | 0.046 | 0.046 | 0.198±0.02 | 0.199 | 0.183 |
| 74 | 1.136±0.08 | 1.083 | 1.077 | 0.043±0.006 | 0.046 | 0.047 | 0.190±0.018 | 0.203 | 0.184 |
| 75 | 1.086±0.12 | 0.898 | 1.054 | 0.045±0.007 | 0.048 | 0.047 | 0.182±0.023 | 0.160 | 0.180 |
| 80 | 0.932±0.08 | 0.920 | 0.962 | 0.044±0.005 | 0.052 | 0.051 | 0.174±0.018 | 0.172 | 0.163 |
| 82 | 0.918±0.08 | 0.937 | 0.986 | 0.049±0.006 | 0.053 | 0.055 | 0.151±0.016 | 0.181 | 0.165 |
| 83 | 0.808±0.075 | 0.990 | 0.953 | 0.049±0.005 | 0.055 | 0.053 | 0.160±0.016 | 0.165 | 0.162 |

**Table 3.** Comparison of our experimental results for relative intensities with theoretical values at an excitation energy of 23 keV.

| $Z$ | $I(L_\beta/L_\alpha)$ | | | $I(L_\gamma/L_\alpha)$ | | | $I(L_l/L_\alpha)$ | | |
|---|---|---|---|---|---|---|---|---|---|
| | Present experiment | Puri[10] | Campbell[9] | Present experiment | Puri[10] | Campbell[9] | Present experiment | Puri[10] | Campbell[9] |
| 62 | 0.188±0.02 | 0.208 | 0.206 | 1.114±0.09 | 1.123 | 1.166 | 0.032±0.008 | 0.040 | 0.041 |
| 64 | 0.209±0.02 | 0.211 | 0.214 | 1.248±0.09 | 1.131 | 1.193 | 0.039±0.009 | 0.041 | 0.041 |
| 65 | 0.198±0.028 | 0.209 | 0.215 | 1.254±0.10 | 1.134 | 1.217 | 0.039±0.012 | 0.041 | 0.042 |
| 73 | 0.183±0.018 | 0.216 | 0.200 | 1.163±0.09 | 1.146 | 1.148 | 0.041±0.006 | 0.046 | 0.046 |
| 74 | 0.173±0.017 | 0.221 | 0.202 | 1.092±0.086 | 1.148 | 1.146 | 0.047±0.007 | 0.047 | 0.047 |
| 75 | 0.161±0.017 | 0.166 | 0.197 | 1.031±0.08 | 0.917 | 1.118 | 0.050±0.008 | 0.048 | 0.047 |
| 80 | 0.159±0.017 | 0.178 | 0.172 | 0.862±0.08 | 0.938 | 0.993 | 0.050±0.006 | 0.052 | 0.051 |
| 82 | 0.143±0.015 | 0.157 | 0.165 | 0.845±0.079 | 0.954 | 0.964 | 0.065±0.008 | 0.053 | 0.053 |
| 83 | 0.153±0.015 | 0.193 | 0.169 | 0.844±0.077 | 0.969 | 0.979 | 0.051±0.006 | 0.054 | 0.053 |

The total uncertainties of the relative intensity values are estimated as the quadrature sum of the uncertainties of the different measured quantities: the number of counts in the peak ($<5\%$), the attenuation correction factor (2%) and, $I_0G\varepsilon$ factor (1%–4%). Since the $L_l$ x-ray intensities are lower in experimental measurements, it should be noted that the value of $I(L_l/L_\alpha)$ is subject to considerable uncertainties.

It can be seen from Tables 2 and 3 and Figs. 2–7 that good agreement was found between the experimental and theoretical relative intensities at both excitation energies (18 keV and 23 keV), although the agreement was better for the relative intensities in the case of 23 keV.

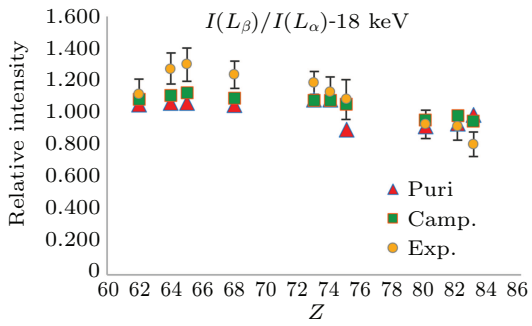



**Fig. 2.** $I(L_\beta/L_\alpha)$ verses atomic number ($Z$) at excitation energy of 18 keV.

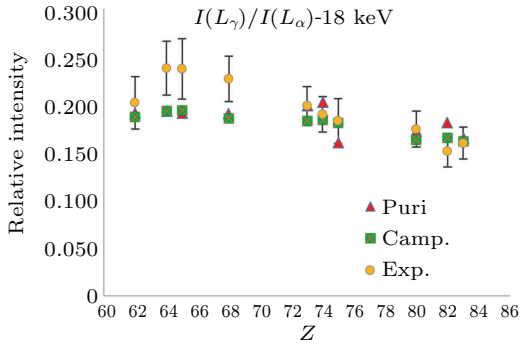



**Fig. 3.** $I(L_\gamma/L_\alpha)$ versus atomic number ($Z$) at excitation energy of 18 keV.

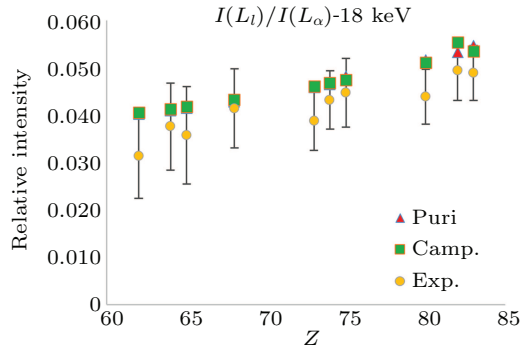



**Fig. 4.** $I(L_l/L_\alpha)$ versus atomic number ($Z$) at excitation energy of 18 keV.

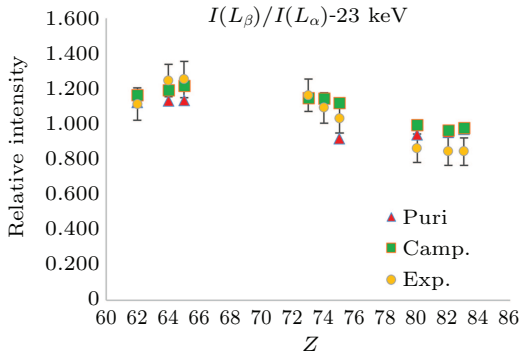



**Fig. 5.** $I(L_\beta/L_\alpha)$ versus atomic number ($Z$) at excitation energy of 18 keV.

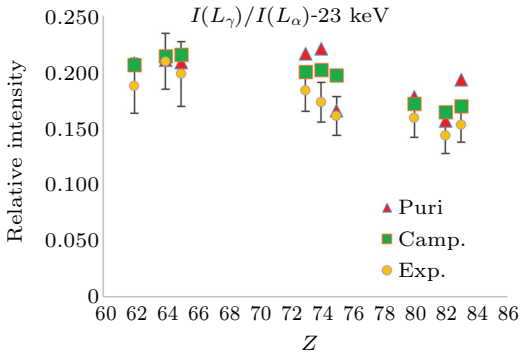



**Fig. 6.** $I(L_\gamma/L_\alpha)$ versus atomic number ($Z$) at excitation energy of 23 keV.

Figures 1–6 show that the present experimental results are closer to the calculated values of Campbell than to the Puri values. The average relative deviation between the measured experimental values of relative intensities $I(L_l/L_\alpha)$, $I(L_\beta/L_\alpha)$ and $I(L_\gamma/L_\alpha)$ and theoretical values of Puri *et al.*[10] at 18 keV were found to be $\sim$ 13%, $\sim$ 12% and 12%, respectively, and for Campbell[9] $\sim$ 9%, $\sim$ 7% and 10%, respectively.

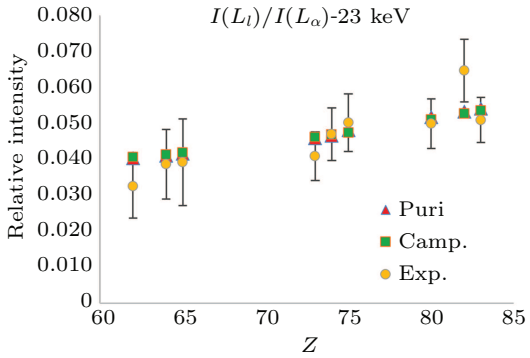



**Fig. 7.** $I(L_l/L_\alpha)$ versus atomic number ($Z$) at excitation energy of 23 keV.

In the case of 23 keV the corresponding values for Puri were $\sim$ 9%, $\sim$ 7% and 10%, respectively, and for Campbell $\sim$ 6%, $\sim$ 10% and 3%, respectively.

Therefore, the experimental results are generally consistent with the theoretical results obtained using the recommended values of $L$-subshell fluorescence yield and CK probabilities by Campbell at both excitation energies (18 keV and 23 keV).

## Acknowledgements

The authors are grateful to Dr Messaoud Harfouche for his technical assistance. This work was supported by the Jordan University of Science and Technology (Grant No. 20180167) and the SESAME Synchrotron Center Jordan (Grant No. 20185004).

## References

[1] Schoonjans T, Silversmit G, Vekemans B, Schmitz S, Burghammer M, Riekel C, Brenker F and Vincze L 2012 *Spectrochim. Acta Part B* **67** 32
[2] Darko and Tetteh G 1992 *X-Ray Spectrom.* **21** 111
[3] Rao D, Cesareo R and Gigante G E 1995 *Radiat. Phys. Chem.* **46** 17
[4] Demir L, Han I and Şahin M 2008 *J. Electron Spectrosc. Relat. Phenom.* **162** 44
[5] Alqadi M, Alsenjlawi Y and Alzoubi F 2013 *Radiat. Phys. Chem.* **87** 31
[6] Bansal H, Tiwari M and Mittal R 2017 *Radiat. Phys. Chem.* **139** 22
[7] Ganly B, Haarlem Y and Tickner J 2016 *X-Ray Spectrom.* **45** 233
[8] Hiremath G, Bennal A, Hosamani M, Badiger N, Trivedi A and Tiwari A 2021 *X-Ray Spectrom.* **50** 37
[9] Campbell J 2003 *At. Data Nucl. Data Tables* **85** 291
[10] S. Puri S, Mehta D, Chand B, Singh N and Trehan N 1993 *X-Ray Spectrom.* **22** 358
[11] Harfouche M, Abdellatief M, Momani Y, Abbadi A, Al Najdawi M, Al Zoubi M, Aljamal B, Matalgah S, Khan L, Lausi A and Paolucci G 2022 *J. Synchrotron Rad.* **29** 1107
[12] Close D, Bearse, Malanify J and Umbarger C 1973 *Phys. Rev. A* **8** 1873
[13] Scofield J H 1973 *Theoretical photoionization cross sections from 1 to 1500 keV*, Lawrence Livermore Laboratory Report No, UCRL-51326
[14] Krause M O, Nestor C W, Sparks C J, Ricci E 1978 *X-ray fluorescence cross sections for K and L x rays of the elements*, Oak Ridge National Lab. Report No ORNL-5399 ORNL-5399
[15] Scofield J H 1974 *At. Data Nucl. Data Tables.* **14** 121
[16] Puri S, Chand B, Mehta D, Garg M L, Singh N and Trehan P N 1995 *At. Data Nucl. Data Tables* **61** 289
[17] Berger M J, Hubbell J H, Seltzer S M, Chang J, Coursey J S, Sukumar R, Zucker D S and Olsen K 2010 *XCOM: Photon Cross Section Database* (version 1.5)